Impact of cementite tortuosity on hydrogen diffusion in pearlitic steels

C. Forot[a], *E. Legrand*[b], *E. Roguet*[c], *J. Creus*[b], *J. Kittel*[a], *X. Feaugas*[b]

[a] *IFP Energies Nouvelles, Rond-point de l'échangeur de Solaize, 69360 Solaize, BP 3, France*
[b] *LaSIE, UMR CNRS 7356, Université de La Rochelle, Bat. Marie Curie, Av. Michel Crepeau, 17042 La Rochelle, France*
[c] *IFP Energies Nouvelles, 1 et 4 avenue de Bois-Préau, 92852 Rueil-Malmaison, France*

Summary

Hydrogen diffusion in two low carbon steels with ferrite-pearlite or purely pearlitic microstructures was studied with hydrogen permeation method. Strong differences in hydrogen permeation transients were observed. A much higher time lag for hydrogen diffusion is obtained for the purely pearlitic steel, which could not be explained with conventional hydrogen diffusion/trapping models. A new model, combining hydrogen diffusion/trapping and geometrical tortuosity of microstructure proved much better adequacy with experimental results.

1 Introduction

It is well known that interactions between hydrogen and steel are sensitive to the microstructure. Many studies relate the impact of microstructure phases (bainite, ferrite, pearlite, austenite or martensite) on the hydrogen diffusion and trapping in steel, as shown by recent publications [1, 2] on the subject. Major differences are observed for steels with different crystal structures. Austenitic steels, with face centred cubic (FCC) structure; always exhibit much higher hydrogen solubility and lower diffusivity [3] than body centered cubic (BCC) steels. Differences between BCC grades (ferrite, bainite, martensite) are usually less pronounced, and associated with different densities of trapping sites [4] (ferrite – cementite interfaces, dislocations…). In general, classical diffusion and trapping models [5-9] correctly describe the behaviour of these steels. However, in multi-phases alloys, very few works question the impact of morphology and connectivity of these phases on diffusion process. Recently, Osman Hoch et al. demonstrate the importance of grain-boundaries connectivity on the diffusion path of polycrystalline structures [10]. This recent work motivates investigation on hydrogen diffusion path of complex pearlitic microstructure.

2 Steels characterization

In the present work, we studied two carbon steels used as flat wires. Their chemical composition is given in Table 1. The only difference between both steels is the carbon content which is 0.35 w% for steel A, and 0.7 w% for steel B. As a consequence, steel B presents higher mechanical properties with an ultimate tensile stress above 1000 MPa compared to 800 MPa for steel A.

Table 1: Chemical composition of tested steels (weight %)

	C	Si	Mn	P	S	Cr	Mo	Ni	Al	Cu
Steel A	0.35	0.22	0.76	0.01	0.005	0.02	<0.005	< 0.02	< 0.03	< 0.02
Steel B	0.71	0.21	0.72	0.01	0.005	0.02	<0.005	< 0.02	< 0.03	< 0.02

Another major difference is the microstructure. A JEOL JEM2010 transmission electron microscope (TEM) with an acceleration voltage of 200 kV was used to characterize both steels. Sample preparation was done by electrolytic polishing as previously described in the literature [11]. TEM show that Steel A is of ferrito-pearlitic type, while steel B presents a fine pearlitic microstructure (Fig. 1). TEM micrographs also show that the cementite fraction in the pearlite zones of both steels is between 13% and 19%. However, steel B is totally pearlitic, while steel A contains around 70 % ferrite grains. High magnification observations at the appropriate tilt angle allowed us to observe dislocations. Image analysis of more than 10 different regions for each steel was performed to determine the density of dislocations using the intersection methods [12]. For steel A, the average dislocation density ρ in the ferrite grains is equal to 8±5 x 1013 m-2 and equal to 1,9±0.7 × 1014 m-2 in pearlitic regions. For steel B, which is 100 % pearlitic, the dislocation density was determined around 3,4±1,0 × 1014 m-2. These values are almost the same for both steels, and result from a high straining process during elaboration.

(a) 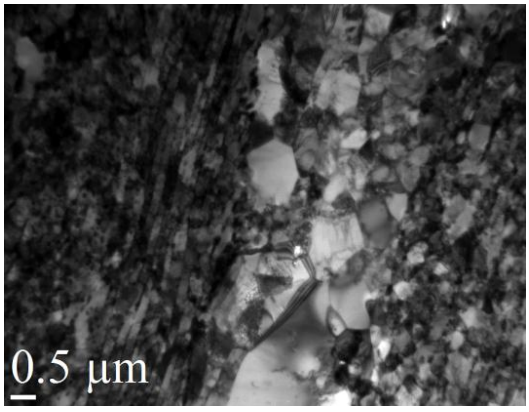

(b) 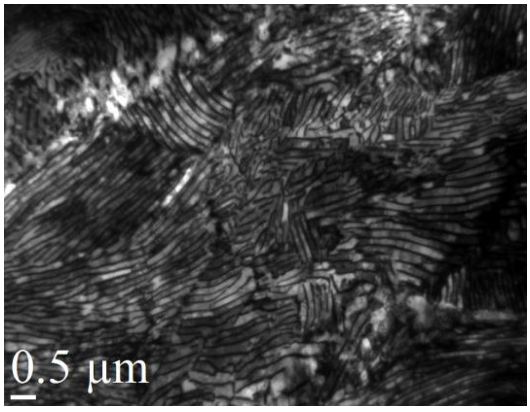

Figure 1: TEM observations of steel A (a) and steel B (b).

3 Study of hydrogen diffusion and trapping

3.1 Experimental set-up

Electrochemical permeation tests were performed with a Devanathan/Stachurski [13, 14] experimental set-up. Jacketed cells were used ensuring a precise control of temperature at 24±1 °C. Permeation membranes were machined from flat wires of steel A or B. Membrane thickness was 2.5 mm and the exposed surface was 0.8 cm². This ratio of radius to thickness is too low to avoid side effects [15]. Nevertheless, this should not affect the comparison between both steels since the geometry is similar. Before each experiment, both faces of the membrane were grinded to SiC paper grit 4000 then degreased in acetone and dried. A thin palladium coating was then electrodeposited on the exit side of the membrane to ensure a complete oxidation of all

hydrogen atoms [11, 16]. A deaerated NaOH 0.1 mol/L solution was used in the detection cell, where hydrogen was oxidized under a fixed potential of 465 mV/SHE filled with 1 M KOH electrolyte. It had previously been verified that no secondary oxidation reaction occurred at this potential. At the beginning of each experiment, filling the charging cell was only realized after a background oxidation current below 0.1 µA/cm² was attained.

The charging cell was filled with a corrosive solution representative of oil production environment. It consisted of a 3.5 % NaCl solution saturated with 0.99 bar CO_2 and 0.01 bar H_2S at ambient pressure. Sodium bicarbonate was added in order to buffer the pH at 4.5.

Before each test, the charging solution was carefully deaerated to less than 10 ppb dissolved O_2 by argon bubbling. The charging cell was also purged with inert gas before introduction of the test solution. Dissolved H_2S and CO_2 were then kept constant by continuous bubbling in the solution during all experiment and the steel surface was kept at free corrosion potential.

3.2 Results and discussion

Figure 2 illustrates typical permeation curves for both steels obtained in charging solution at pH 4.5 with 10 mbar H_2S and 990 mbar CO_2. Although the same corrosion potential was measured for both steels (-670 ± 10 mV vs. Ag/AgCl). Permeation transients showed strong differences between steel A and steel B. The exit delay of hydrogen is much higher for steel B, and its steady-state flux is lower than for steel A. Several other permeation tests were performed at other pH and H_2S partial pressure and the same trend was systematically observed. Qualitatively, this trend may be a result of a lower hydrogen apparent diffusivity (Dapp) for steel B. According to diffusion – trapping models [7, 9], increasing the number of traps directly results in a decrease of Dapp. For ferrite-pearlitic steels, such increase of trap density is often associated [17] to with local trapping at the cementite/ferrite interphases and dislocations density.

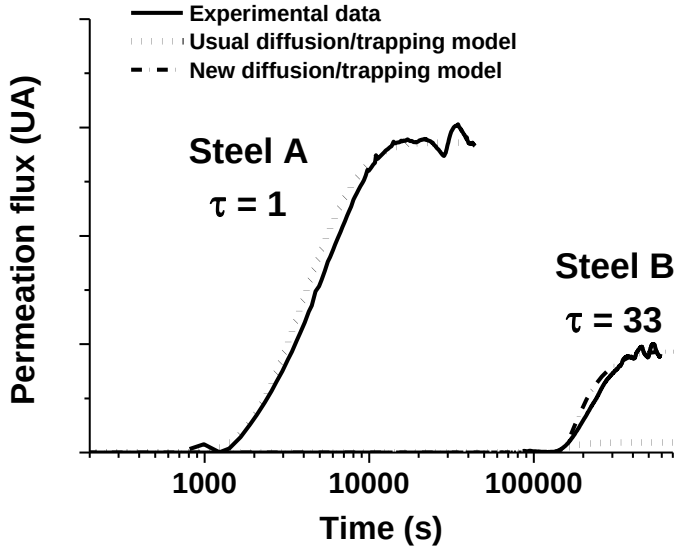

Figure 2: Comparison between the experimental data and the best numerical correlation for both steels. Taking tortuosity into account for steel B.

Permeation transients were therefore analyzed with a diffusion/trapping model [5, 6, 9, 18] based on McNabb/Oriani equations. In the case of steel A, the numerical model fits well to experimental data. On the contrary, the behavior of steel B could not be correctly represented with this model. Indeed, as illustrated on Figure 2, this model strongly underestimates the increase of hydrogen permeation current during the transient. For pearlitic steels, it is often considered [19] that cementite acts as a diffusion barrier. Hydrogen diffusion thus proceeds only through the ferrite phase. Due to the continuous aspect of cementite bands (Figure 1), a large increase of diffusion path is created for steel B. In order to capture this effect [19, 20], a tortuosity parameter (τ) was defined as the ratio between the length of the real hydrogen path and the length of the shortest path, i.e., the membrane thickness.

From TEM micrographs, we estimated the average tortuosity of steel B to be between 20 and 35. Combining geometrical tortuosity with the previous diffusion – trapping model, hydrogen diffusion was modeled with the finite element analysis software Comsol Multiphysics, associated with the numerical computing environment MATLAB. For hydrogen, diffusion was considered to proceed only by lattice diffusion in the ferrite phase, with a path increased by tortuosity effect. The diffusion equations used are based on Fick's laws. In order to account for hydrogen traps, modifications of diffusion equations were applied, identically as in the work of McNabb, Foster, Oriani and Krom [5, 6, 7], later modified by several authors [9, 18, 21, 22, 23].
A free triangular mesh was used for the calculations, and the problem was solved using the Parallel Sparse Direct And Multi-Recursive Iterative Linear Solvers package PARDISO [24]. The thickness of the membrane was e = 2.5 mm. The lattice sites density N_L was taken equal to 2×105 mol/m3 [7, 8]. A trap binding energy of -0.3 eV was used [9, 18], in order to consider deep hydrogen trapping.

The effect of tortuosity on permeation transients is illustrated on Figure 3 for different tortuosity values. Tortuosity raises drastically the hydrogen delay to exit the membrane, and the steady-state flux is also strongly decreased. To emphasize the effects of the tortuosity, we present in Figure 4 the variation of the normalized exit-side delay of permeation curves as a function of the square of tortuosity obtained using FEM calculation. A linear relation clearly appears between both independently to the set of diffusion coefficient and trapping parameters. In other words, t10% is the sum of the delay due to hydrogen trapping and the delay due to the tortuosity. This last result provides a simple method to extract diffusion coefficient from experimental data considering tortuosity of diffusion path.

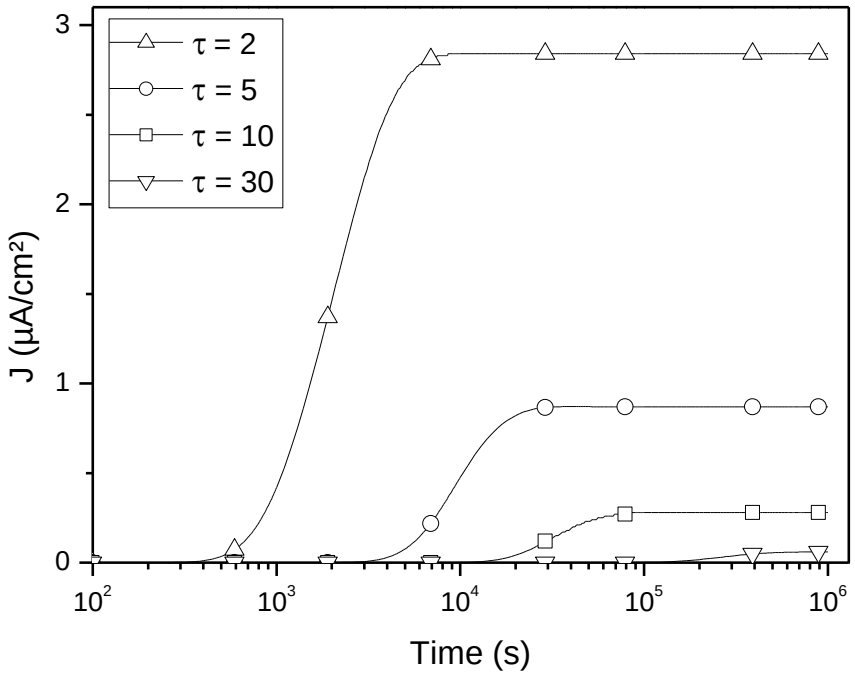

Figure 3: Effect of the tortuosity of hydrogen path on a permeation transient (other parameters equals).

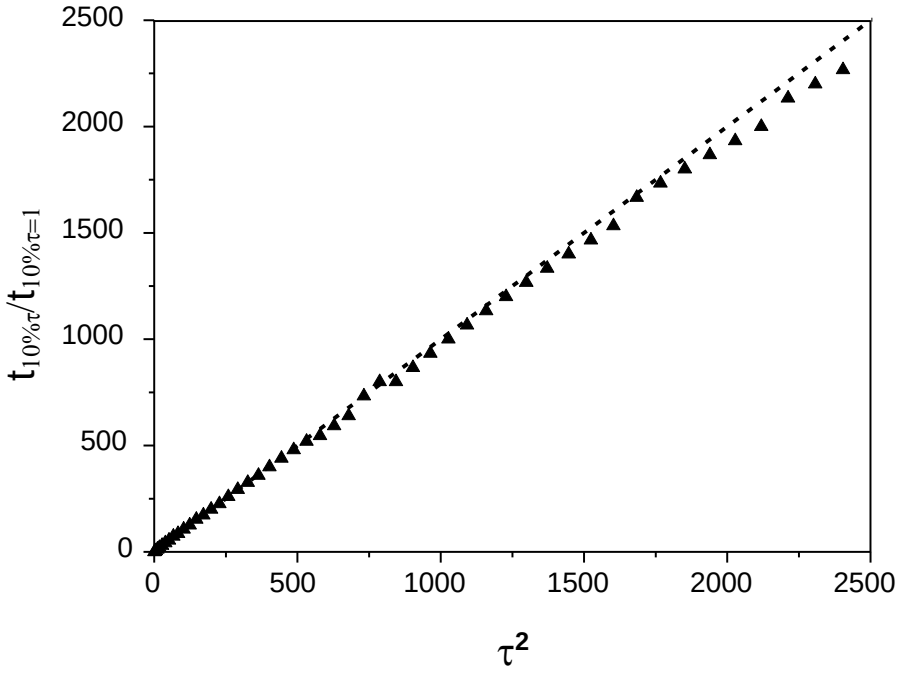

Figure 4: Correlation between the standard time lag and the time lag of a tortuous material depending on the tortuosity value

4 Conclusion

We have considered hydrogen diffusion in two different BCC steels, with ferrite-pearlitic or purely pearlitic microstructures. Both steels exhibited strong differences in permeation transients, with a much larger time lag for the pearlitic grade. Hydrogen diffusion behavior of the ferrito-pearlitic steel could well be modeled by usual diffusion-trapping models from the literature. On the contrary, these models were not capable to represent correctly the behavior of steel B. A new model, including an increase of hydrogen diffusion path associated with the pearlitic microstructure was proposed. Numerically, we observed a remarkable correlation with the experimental permeation data, non-attainable using only a classic diffusion and trapping model. This new model allows determining more accurately the effective hydrogen diffusion coefficient in the steel, as well as the trap density and hydrogen subsurface concentration.

References

[1] W.K. Kim, S.U. Koh, B.Y. Yang, K.Y. Kim, Effect of environmental and metallurgical factors on hydrogen induced cracking of HSLA steels, Corros. Sci. 50 (2008) 3336.

[2] F. Huang, J. Liu, Z.J. Deng, J.H. Cheng, Z.H. Lu, X.G. Li, Effect of microstructure and inclusions on hydrogen induced cracking susceptibility and hydrogen trapping efficiency of X120 pipeline steel, Mat. Sci. Eng. A. 527 (2010) 6997.

[3] J. Völkl, G. Alefeld, Diffusion of hydrogen in metals, Appl. Phy. 28 (1978) 321.

[4] M.I. Luppo, J. Ovejero-Garcia, The influence of microstructure on the trapping and diffusion of hydrogen in a low carbon steel, Corros. Sci. 32 (1991) 1125.

[5] A. Mc Nabb and P.K. Foster, A new analysis of the diffusion of hydrogen in iron and ferritic steels, Trans. Metall. Soc. AIME, 227 (1963) 618.

[6] R.A. Oriani. The diffusion and trapping of hydrogen in steel, Acta Metall. 18 (1970) 147.

[7] A.H.M. Krom, A.D. Bakker, Hydrogen trapping models in steel, Metall. Mater. Trans. B 31 (2000), 1475.

[8] S. Frappart, X. Feaugas, J. Creus, F. Thebault, L. Delattre, H. Marchebois, Study of the hydrogen diffusion and segregation into Fe–C–Mo martensitic HSLA steel using electrochemical permeation test, J. Phys. Chem. Solids 71 (2010) 1467.

[9] E. Legrand, J. Bouhattate, X. Feaugas, H. Garmestani, Numerical analysis of the influence of scale effects and microstructure on hydrogen diffusion in polycrystalline aggregates, Int. J. Hydrogen Energ. 37 (2012) 13574.

[10] B. Osman Hoch, A. Metsue, J. Bouhattate, X. Feaugas, Effects of grain-boundary networks on the macroscopic diffusivity of hydrogen in polycrystalline materials, Comp. Mater. Sci. 97 (2015) 276.

[11] S. Frappart, A. Oudriss, X. Feaugas, J. Creus, J. Bouhattate, F. Thebault, L. Delattre, H. Marchebois, M. Hörstemeier, Study of the Hydrogen diffusion and trapping mechanisms into quenched and tempered HSLA steels using electrochemical permeation technique, Scripta Mater. 65 (2011) 859.

[12] Hirsch P.B., Howie A., Nicholson R., Pashley D.W., and Whelam M.J, Electron microscopy of thin crystals, J. Nucl. Mater. 21 (1967) 356.

[13] M.A.V. Devanathan, Z. Stachurksi, The mechanism of hydrogen evolution on iron in acid solutions by determination of permeation rates, J. Electrochem. Soc. 111 (1964) 619.

[14] T. Zakroczymski, Adaptation of the electrochemical permeation technique for studying entry, transport and trapping of hydrogen in metals, Electrochim Acta. 51 (2006) 2261.

[15] ASTM G148-97(2003), Standard Practice for Evaluation of Hydrogen Uptake, Permeation, and Transport in Metals by an Electrochemical Technique, ASTM International, West Conshohocken, PA, 1997, www.astm.org

[16] P. Manolatos, M. Jerome, A thin palladium coating on iron for hydrogen permeation studies, Electrochim Acta. 41 (1996) 359.

[17] H. Hagi, Hydrogen embrittlement of mild steel charged cathodically with hydrogen, Mater. T. JIM, 35 (1994) 168.

[18] J. Bouhattate, E. Legrand, X. Feaugas, Computational analysis of geometrical factors affecting experimental data extracted from hydrogen permeation tests: I - Consequences of trapping, Int. J. Hydrogen Energ. 36 (2011) 12644.

[19] L. Tau, S.L.I. Chan, Effects of ferrite/pearlite alignment on the hydrogen permeation in a AISI 4130 steel, Mater. Lett. 29 (1996) 143.

[20] S.L.I. Chan, Hydrogen trapping ability of steels with different microstructures, J. Chinese Inst. Engrs 22 (1999) 43.

[21] J. Svoboda, F.D. Fischer, Modelling for hydrogen diffusion in metals with traps revisited, Acta Mater. 60 (2012), 1211.

[22] F.D. Fischer, G. Mori, J. Svoboda, Modelling the influence of trapping on hydrogen permeation in metals, Corros. Sci. 76 (2013), 382.

[23] E. Legrand, J. Bouhattate, X. Feaugas, Generalized model of desorption kinetics: Characterization of hydrogen trapping in a homogeneous membrane, Int. J. Hydrogen Energ. 39 (2014) 2430.

[24] O. Schenk, A. Waechter, M. Hagemann, Matching-based preprocessing algorithms to the solution of saddle-point problems in large-scale nonconvex interior-point optimization, J. Comput. Optim. Appl. 36 (2007) 321.